



## RESEARCH ARTICLE

10.1029/2018JD029040

## Generation of Seed Electrons by Extensive Air Showers, and the Lightning Inception Problem Including Narrow Bipolar Events

## Key Points:

- We calculate the probabilities of extreme densities of thermal electrons in extensive air showers
- The spatial distribution of the electrons might explain correlations in lightning inception (Rison et al., 2016)

Casper Rutjes<sup>1</sup> , Ute Ebert<sup>1,2</sup> , Stijn Buitink<sup>3</sup> , Olaf Scholten<sup>3,4</sup> , and Thi Ngoc Gia Trinh<sup>4,5</sup>

<sup>1</sup>Multiscale Dynamics group, Centrum Wiskunde & Informatica (CWI), Amsterdam, Netherlands, <sup>2</sup>Department of Applied Physics, Eindhoven University of Technology, Eindhoven, Netherlands, <sup>3</sup>Department of Physics, Vrije Universiteit Brussel, Brussels, Belgium, <sup>4</sup>KVI-CART, University of Groningen, Groningen, Netherlands, <sup>5</sup>Department of Physics, School of Education, Can Tho University, Can Tho, Vietnam

## Supporting Information:

- Supporting Information S1

## Correspondence to:

U. Ebert,  
u.ebert@tue.nl

## Citation:

Rutjes, C., Ebert, U., Buitink, S., Scholten, O., & Trinh, T. N. G. (2019). Generation of seed electrons by extensive air showers, and the lightning inception problem including narrow bipolar events. *Journal of Geophysical Research: Atmospheres*, 124, 7255–7269. <https://doi.org/10.1029/2018JD029040>

Received 21 MAY 2018

Accepted 7 MAY 2019

Accepted article online 3 JUN 2019

Published online 8 JUL 2019

**Abstract** Lightning streamers and leaders need thermal electrons to initiate, but free electrons are extremely rare in the wet air of a thundercloud. Here we analyze the probabilities that high electron densities occur in extensive air showers. We argue that relevant air showers are created by cosmic particles with energies between  $10^{15}$  and  $10^{17}$  eV impinging onto our atmosphere. We simulate a large number of air showers and perform a stochastic analysis of their results. We present the available densities of thermal electrons as a function of altitude, time interval, and considered area, while neglecting effects of local electric fields. We find that free electron densities at altitudes between 5 and 13 km can reach values of order  $10^3$  cm<sup>-3</sup>, but only in shower cores with a radius on a centimeter scale. Above 6 km, the availability of extreme free electron densities decreases significantly with increasing altitude. Recent measurements by Rison et al. (2016, <https://doi.org/10.1038/ncomms10721>) indicate that several streamers must have been triggered simultaneously during discharge inception, and we suggest that an extensive air shower could have been the trigger. Rison's measurements show further that the streamers are laterally separated by several tens of meters, so they must have been triggered by electron densities as low as 1 cm<sup>-3</sup>. Such low electron densities demand a stochastic approach to streamer initiation near hydrometeors.

## 1. Introduction

Thunderclouds produce strong electric fields. However, the electric fields measured before discharge activity starts are too low for classical breakdown of air (Marshall et al., 1995, 2005; Stolzenburg et al., 2007). The solution offered in model simulations by Liu et al. (2012), Sadighi et al. (2015), Dubinova et al. (2015), and Babich et al. (2016, 2017) and in older references quoted by these authors is that hydrometeors due to their shape and high dielectric permittivity or also due to their net electric charge locally enhance the ambient electric field to values above the classical breakdown field. However, the configuration of the electric field near a hydrometeor alone does not yet determine electric breakdown, but thermal free electrons are required in the critical volume as well. (Electrons with energies from fractions to tens of electron volts (eV) are called thermal in the community.)

Thermal free electrons are very rare in the humid environment of a thundercloud (Dubinova et al., 2015), though they are continuously refreshed by background radiation, that is, by cosmic rays and by radioactive decay at a rate of the order of  $10$  cm<sup>-3</sup>·s<sup>-1</sup> (Usoskin et al., 2009). But free electrons attach to electronegative molecules like oxygen on a time scale of 50 ns (Pancheshnyi, 2013) to form O<sub>2</sub><sup>-</sup>. These ions in turn act as condensation nuclei for ion-water clusters O<sub>2</sub><sup>-</sup>(H<sub>2</sub>O)<sub>n</sub> that form within microseconds (Gallimberti, 1979). This reaction chain efficiently removes free electrons from the cloud, such that the steady state of the free electron density is only  $5 \times 10^{-7}$  cm<sup>-3</sup>, which makes streamer initiation from a hydrometeor extremely unlikely.

As we already argued in Dubinova et al. (2015), the only way to get a significant free electron seed is by a very energetic cosmic ray impinging on the atmosphere and creating an extensive air shower (EAS). In the earlier work it was shown that the free electron densities produced in the core of an EAS can be 9 orders of magnitude larger than in steady state, and they occur only rarely. In the present work we calculate the availability of extreme electron seeds in thunderclouds, by performing a probability analysis of EAS events. We stress that these densities are created independently of the local electric fields, but that relativistic

©2019. The Authors.

This is an open access article under the terms of the Creative Commons Attribution-NonCommercial-NoDerivs License, which permits use and distribution in any medium, provided the original work is properly cited, the use is non-commercial and no modifications or adaptations are made.

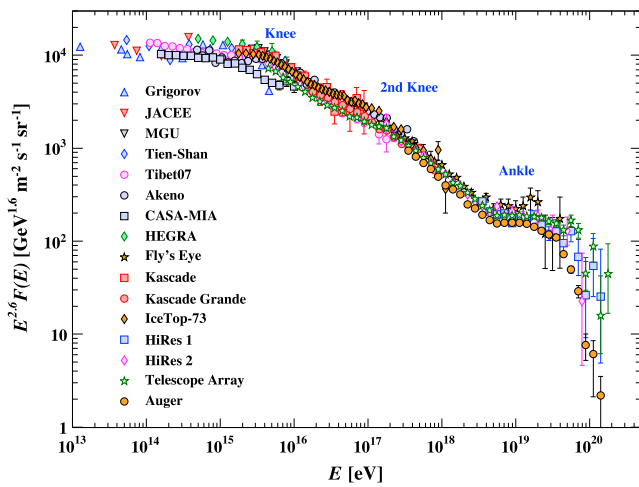


**Figure 1.** The flux of cosmic particles impinging on our atmosphere as a function of the particle energy  $E$  (eV), rescaled with a factor of  $E^{2.6}$ . The data are derived from air shower measurements. The flux  $F(E)dE$  is the particle number per area, time, solid angle, and size of the energy interval. The figure is reproduced from Figure 29.8 in the 2016 review of the Particle Data Group (Patrignani et al., 2016), and it is unchanged in the 2018 edition of the review.

runaway electron avalanches in thunderstorm electric fields can further augment the densities of thermal electrons.

The quest for extreme electron seeds from EASs has recently become even more timely, as Rison et al. (2016) interpret their measurements of fast positive breakdown as a volumetric system of streamers. This phenomenon occurs during so-called narrow bipolar events (NBE) at the beginning of discharge activity in a cloud. Rison et al. argue that multiple streamers could initiate from multiple hydrometers in close proximity and synchronously on a time scale of nanoseconds. The added currents of multiple streamers could initiate a longer leader discharge and create a radio signal strong enough to be measured from the ground.

Here we study the probability of high electron densities at a given radius and the probability of large shower radii for given electron density, created by EASs. The study is organized as follows. We first introduce the physical system in section 2, which are the EASs producing free electrons. In section 3 we explain our methodology. After presenting the results in section 4, we discuss their implications in the context of lightning initiation in section 5. We conclude in section 6 with an outlook on further studies related to this work.

## 2. The Physical System

### 2.1. Cosmic Rays and Induced Extensive Air Showers (EASs)

Our atmosphere is bombarded by cosmic particles (commonly called cosmic rays). Figure 1 shows the flux spectrum of cosmic rays as a function of particle energy. The flux (in a particular energy interval) should be interpreted as the average number of cosmic rays per unit of area, time, and solid angle. In the energy interval of  $10^{15}$  to  $10^{17}$  eV relevant for the present study (as we will argue in

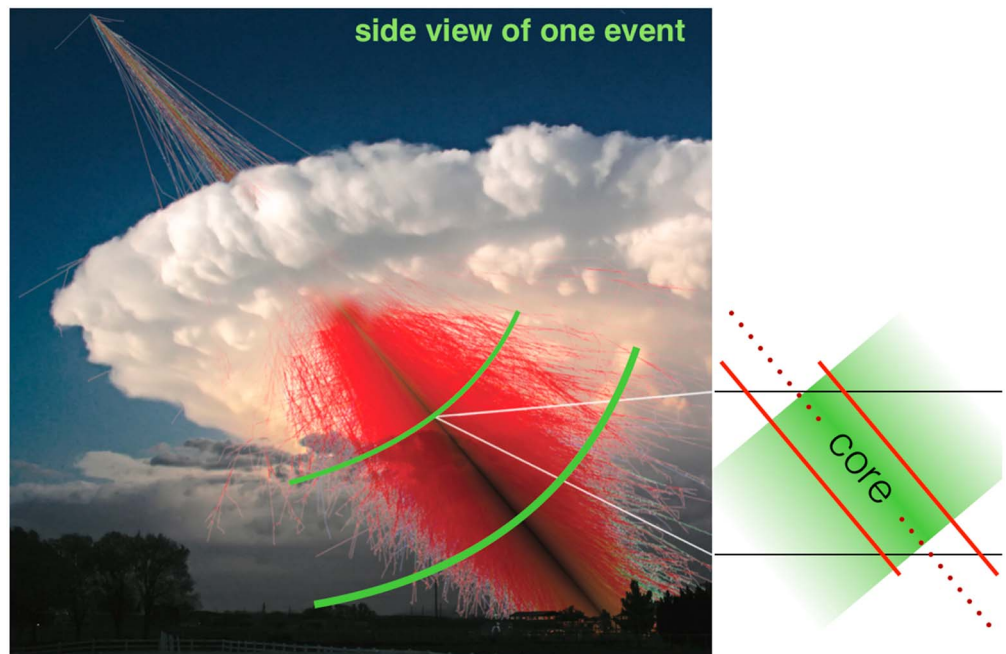


**Figure 2.** Illustration of an extensive particle shower in side view. The red lines indicate the (time integrated) trajectories of the shower particles, and the green lines the particle distributions at particular instances of time. As all particles move essentially with the speed of light, at one instant of time, they form a pancake structure indicated in green; two pancakes at two instances of time are indicated on the left panel. The right panel shows a zoom into one pancake on the shower axis (that is determined by the momentum vector of the initial cosmic ray), showing its spatial extension in green, and the dense core of the shower is here limited by red particle trajectories.

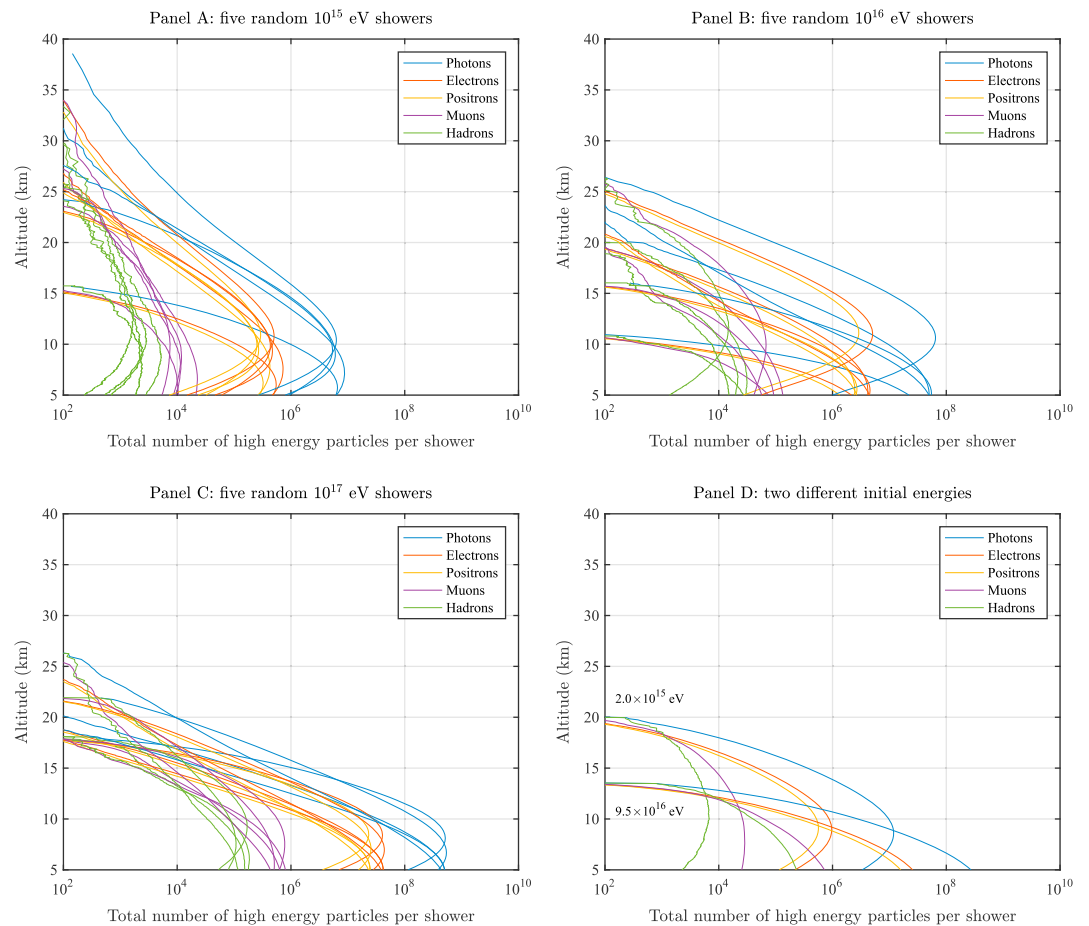


**Figure 3.** Illustration of shower to shower variations, derived with the CORSIKA code described in the next section. (a) Simulations of five different air showers produced always by a primary proton with  $10^{15}$ -eV energy. Plotted is the number of passing extensive air shower particles as a function of altitude. The particles are photons (blue), electrons (red), and positrons (yellow) with energy above 50 keV, muons above 30 MeV (purple), and hadrons above 300 MeV (green). (b and c) The same for cosmic rays of  $10^{16}$  and  $10^{17}$  eV, respectively. (d) The huge shower to shower variations: the shower with a much lower primary energy in this particular example creates much larger particle numbers above 10-km altitude—this behavior is not typical but possible.

section 2.5), the flux is uniformly distributed per solid angle (i.e., isotropic) and it follows a Poisson distribution in space and time. It should be noted that the distribution is uniform only in some intermediate energy range: The flux of cosmic rays from the Sun (with energies below about  $10^{11}$  eV) is strongest near the poles because of the geomagnetic field, and it changes with the day and night cycle and the solar 11-year cycle, and for particles with energy above  $10^{18}$  eV recently some anisotropy has been found (Gaisser et al., 2016; Patrignani et al., 2016).

The spectrum in Figure 1 steepens around the energy of  $10^{15}$  eV, called the *knee* which reflects the fact that most cosmic accelerators in the galaxy cannot achieve higher energies. Beyond the so called *ankle*, at  $3.1 \times 10^{18}$  eV, extragalactic flux begins to dominate over the galactic flux (Patrignani et al., 2016).

Once a high-energy cosmic ray enters the atmosphere and collides with an air molecule, it creates a cascade of secondary elementary particles, as illustrated in Figure 2. Basically, every collision of a secondary particle with still sufficient kinetic energy is creating new secondary particles by converting energy into mass. This cascade will continue down to MeV, creating electrons and positrons which are the stable elementary particles with the smallest rest mass, leaving the essentially noninteracting neutrinos out of consideration; this is called an EAS. Particles in the EAS have typically much larger kinetic energies than their rest mass,

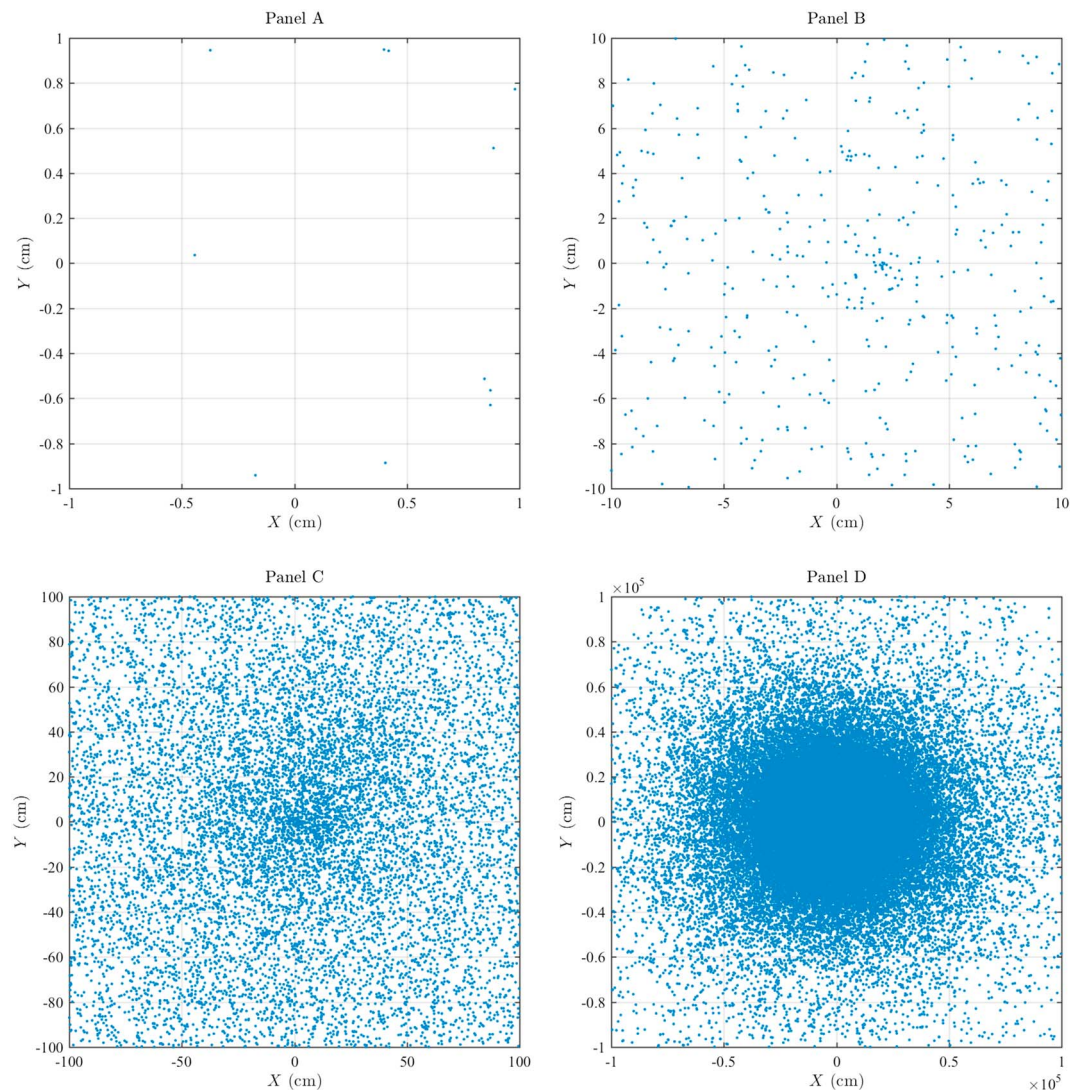


**Figure 4.** Positions of electrons and positrons with energies above 50 keV when they cross through the plane perpendicular to the shower at 6-km altitude. The shower was generated by a  $10^{16}$ -eV proton with zero inclination. Panels (a) to (d) show the same data but zooming into the scale of  $\pm 1$  cm,  $\pm 10$  cm,  $\pm 1$  m, and  $\pm 1$  km, respectively, around the shower axis. The cylindrical symmetry is clearly visible in panel (d), but for radii below 10 cm the total number of particles in the plot becomes too small to see any structure. The results were derived with the CORSIKA code described in the next section.

so they move relativistically, essentially with the speed of light. Figure 2 illustrates the particle trajectories in the EAS in red. The EAS at one instant of time should be thought of as a thin pancake structure moving with almost the speed of light toward the ground (two snapshots are illustrated in green). The particle flux in this pancake is most dense around the symmetry axis of the shower, called the core of the EAS.

The relativistic shower particles leave a trail of lower-energy particles behind, including electrons with energies in the eV range that can play a role in discharge inception. Obviously, these slower particles cannot have an influence on the EAS evolution itself. We will come back to them in section 2.3.

## 2.2. The Randomness of EASs

The energy of the cosmic ray is only one parameter that determines the evolution of the EAS, and there are large shower to shower variations even when this parameter is fixed. They are caused by the random inclination of the particle incidence and by the first 100 or so collisions; thereafter self-averaging will take place. These variations are illustrated in Figures 3a–3c where in each panel the longitudinal evolution of

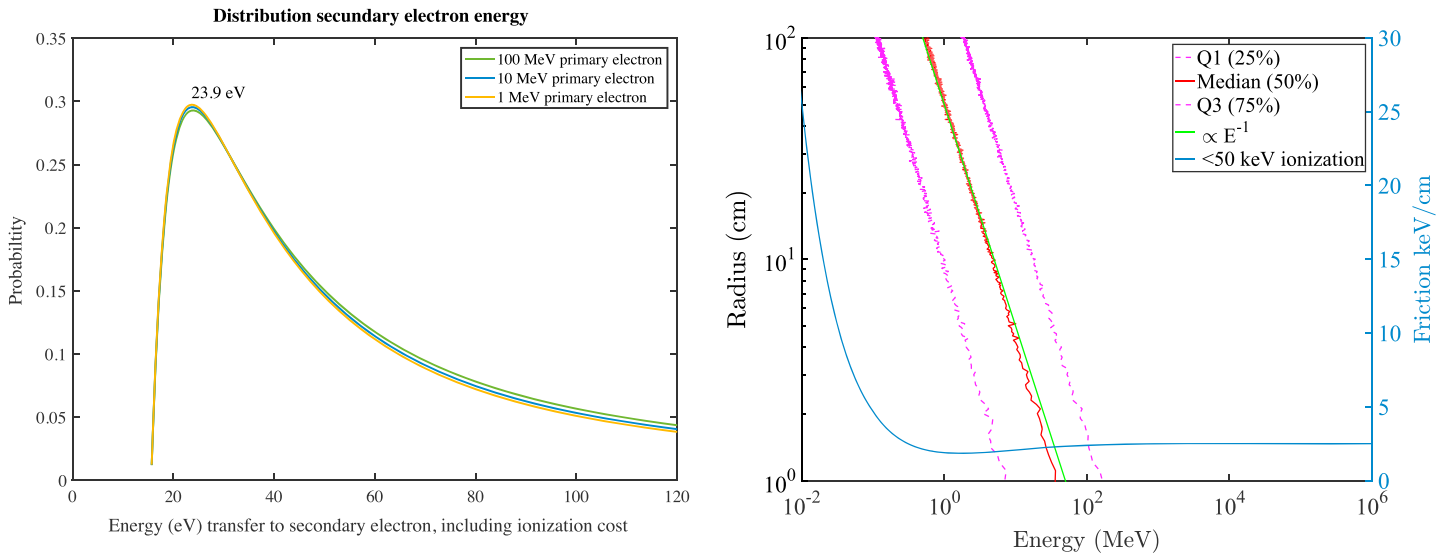


**Figure 5.** (left panel) Distribution of the energy losses of EAS electrons with 1-, 10-, or 100-MeV energy (color coded) in impact ionization events according to the Relativistic Binary Encounter Bethe (RBEB) theory (Santos et al., 2003). The energy loss of the relativistic EAS electron has to exceed the binding energy of the secondary electron in the molecule; this is why the energy spectrum in the panel is bounded on the left. (right panel) The energy distributions of electrons and positrons in EASs show a typical pattern as a function of radius; the red lines indicate where 25%, 50%, and 75% of the population is in energy (i.e., it is a boxplot). The subcollisional friction (blue line), that is, the energy into ionizations below 50 keV, is for electron energies above 0.1 MeV independent of kinetic energy (please note the linear scale). The average friction used in this study is equal to 2.5 keV/cm. Friction is displayed here for an air density of  $1.293 \cdot 10^{-3}$  g/cm<sup>3</sup> corresponding to 1 bar and 273 K. It should be noted that almost all EAS electrons are above 1 MeV and that above 1 MeV the friction is nearly independent of electron energy. EAS = extensive air shower.

five different proton-generated EASs is given for a fixed primary proton energy. Shown are the numbers of passing photons, electrons, and positrons above 50-keV energy, and of muons above 30 MeV and hadrons above 300 MeV as a function of altitude. The three most significant EAS particle types are photons, electrons, and positrons. (Note the logarithmic density scale of the plot.) Electrons and positrons are produced in equal numbers by pair production but with a small surplus of electrons due to sporadic hard impact ionization.

The longitudinal shower projection in Figure 3 looks like a bell-shaped structure, where the altitude of the shower maximum decreases on average with increasing primary energy, because higher-energy particles penetrate deeper into the atmosphere before their first interaction with an air molecule. For the average EAS the maximal number of particles in the shower scales roughly linearly with primary energy. There exists “shower universality” which implies that given the point of first interaction the number of particles as a function of penetration depth is determined rather well (Lafebre et al., 2009; Lipari, 2016).

Due to the large shower to shower variations, for a given altitude the number of particles is not uniquely related to the primary particle energy. This is illustrated in Figure 3d with two handpicked showers: Even though the  $9.5 \times 10^{16}$  eV shower has more particles than the  $2 \times 10^{15}$  eV shower at their respective shower maxima, above 8-km altitude the  $2 \times 10^{15}$  eV shower has more particles than the  $9.5 \times 10^{16}$  eV one.

Figure 4 shows an example of the positions of electrons and positrons with energies above 50 keV (later called EAS particles) when they pass through the plane perpendicular to the shower at 6-km altitude. The shower was generated by a proton of  $10^{16}$  eV energy impinging vertically, and the origin of the coordinate system is the shower axis. The panels zoom into different scales of the shower core. In Figure 4d on a kilometer scale the cylindrical symmetry is clearly visible, but in Figure 4a on a centimeter scale, the particle number is too low to see any structure.

### 2.3. Energy Decoupling: The eV Electrons Generated by the EAS

While the pancake of particles in the EAS rushes downward with nearly the speed of light, all particles collide with air molecules and lose energy, for example, by ionization of air molecules. Sporadically they transfer significant energy to a bound electron promoting it to the EAS population, but most of the time they only free an electron and transfer up to a few tens of eV of energy; the probability distribution of energy loss of the primary particles by electron impact ionization is illustrated in the left panel of Figure 5. These

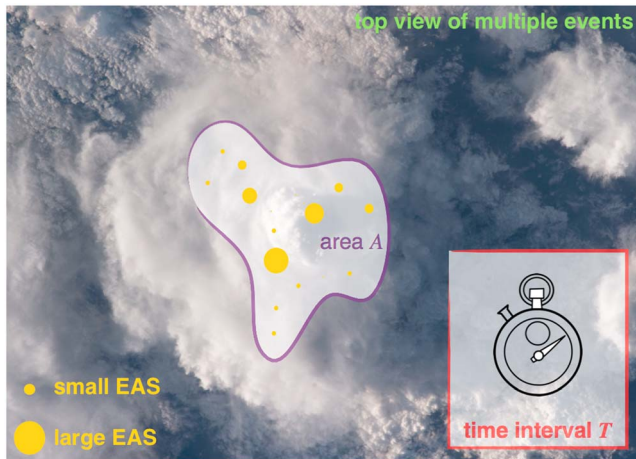


**Figure 6.** In the top view of a thundercloud, an area  $A$  and a time interval  $T$  are marked;  $A \cdot T$  will be denoted as the system size. Within this area and time, several EAS (marked as yellow spots) can pass at random location and time and with random size; they are statistically independent of each other, and they can be assumed to be nonoverlapping, also due to their short duration. We calculate the maximal strength of a shower to be expected, where the maximum is taken over all showers within the system size, and the strength is, for example, a certain electron density within a given radius. EAS = extensive air shower.

collisions create electrons with energy in the eV range (the energy loss of the primary particle minus the binding energy in the molecule) that are finally available as seed electrons for discharge inception.

Therefore, the system can be decoupled into

- *EAS particles*: relativistic electrons and positrons, moving nearly with the speed of light, with energies above 1 MeV.
- *Seed electrons*: free electrons left behind by an EAS, mostly with tens of eV energies, seeding classical breakdown.

The EAS particles create seed electrons, but the energy losses of the EAS particles can be taken into account by averaging over the seed particle creation, so the seed electron distribution does not couple back on the EAS particles. This is due to two effects: First, as the energy loss  $F$  per collision is so much smaller than the kinetic energy of the EAS particle, it is fair to approximate it as a continuous energy loss per unit of length or friction for the EAS particle. (Note that “friction” is used as energy loss per length in the high-energy community, so it does not have the unit of a force.) The friction  $F$  of an EAS electron due to producing secondary electrons below 50 keV is given in blue in the right panel of Figure 5. Second, as shown in the left panel of Figure 5, the ionization cross section to produce electrons below 50 keV is essentially independent of the energy of the EAS particle, as long as it exceeds about 0.5 MeV.

It turns out that only EAS electrons and positrons leave a significant trail of thermalized free electrons behind, even though the flux of EAS photons is roughly 10 times larger, as illustrated in Figure 3. The reason is that the friction of electrons and positrons is almost 6 orders of magnitude larger than that of the photons; that is, they lose much more energy and hence create many more seed electrons. Electrons and positrons leave an approximately equal amount of seed electrons behind. These seed electrons can be approximated as an EAS particle yield  $Y$  per unit of length,

$$Y(h) = F(h)/W = 74 \text{ cm}^{-1} \left( \frac{n_{\text{air}}(h)}{n_{\text{air}}(0)} \right), \quad (1)$$

as function of altitude  $h$ , using an average friction of  $F = 2.5 \text{ keV/cm}$  (see Figure 5) where  $n_{\text{air}}(h)$  is air density at altitude  $h$ , and  $h = 0$  refers to standard temperature and pressure; hence, the yield decreases at higher altitudes  $h$ . In the yield the energy cost per free electron is taken as  $W = 34 \text{ eV}$  from Jesse and Sadauskis (1955), Cole (1969), Knoll (2010), and Dwyer and Babich (2011). Usoskin and Kovaltsov (2006) use a similar value of  $W = 35 \text{ eV}$ .

Finally, as already discussed in section 1, the lifetime of the created seed electrons is limited by electron attachment. A general number for the attachment time cannot be given as it depends on the local electric field, the air density, and the humidity. However, typical attachment times are of the order of tens to hundreds of nanoseconds, much shorter than the times on which the electric field in a thundercloud varies before discharge activity starts. This means that the electric field can be assumed to be static while the seed electrons appear and disappear.

#### 2.4. How to Measure the Probability of an Event

It is important to note that EASs occur at random locations and times, and with random sizes, and that they are statistically independent. This is because independent cosmic particles with random energy, inclination, and first atmospheric interactions impinge on the atmosphere. Therefore, the number of EAS that on average pass through an area is proportional to the area  $A$  and the waiting time  $T$ , that is, only the product of  $A$  and  $T$  determines the likelihood of an event. Area and time interval for EAS are illustrated in Figure 6. We will call  $A \cdot T$  the system size and calculate probabilities for varying system sizes.

Furthermore, due to the short lifetime of the seed electrons until attachment, the probability that the electron densities of two different EASs add up to one larger density can be neglected.

### 2.5. Identifying the Relevant Energy Range of Cosmic Rays

The flux of cosmic rays in Figure 1 decays with energy  $E$  approximately like  $E^{-2.7}$  in the energy range from  $10^{14}$  to  $10^{15}$  eV and like  $E^{-3}$  between  $10^{15}$  and  $10^{17}$  eV. More precisely, in the energy range of  $10^{15}$  to  $10^{17}$  eV the differential flux in energy can be approximated as

$$F_{70^\circ}(E) dE = \frac{13}{\text{km}^2 \text{ s}} \left( \frac{10^{15} \text{ eV}}{E} \right)^3 \frac{dE}{10^{15} \text{ eV}}, \quad (2)$$

with the error nowhere exceeding 25%. Here  $F_{70^\circ}(E) dE = \Omega(70^\circ) F(E) dE$  is the flux  $F(E)dE$  per solid angle of Figure 1 multiplied by a solid angle of  $\Omega(70^\circ) = 2\pi(1 - \cos 70^\circ) \approx 4.1$ . This solid angle corresponds to a cone with an opening angle of  $70^\circ$ ; the size of this opening angle will be motivated in the next section.

The fluxes integrated over different energy intervals  $\int F_{70^\circ}(E) dE$  are approximately

$$\begin{aligned} \frac{6.5}{\text{km}^2 \text{ s}} &= \frac{1}{(400 \text{ m})^2 \text{ s}} && \text{for the energy interval } 10^{15} \text{ eV} \leq E \leq 10^{16} \text{ eV}, \\ \frac{0.065}{\text{km}^2 \text{ s}} &= \frac{1}{15 \text{ km}^2 \text{ s}} && \text{for the energy interval } 10^{16} \text{ eV} \leq E \leq 10^{17} \text{ eV}. \end{aligned} \quad (3)$$

To determine the energy range for the primary cosmic rays appropriate for this study, we have to understand the occurrence rate of interest for thunderstorm phenomena. Following the study of Stolzenburg et al. (1998), thunderstorms come in a variety of sizes and lightning intensities, from small single-celled storms that are generally about 10 km in diameter and have a lifetime of typically 60–90 min, up to supercell storms with a typical horizontal coverage of 250 km<sup>2</sup> and lifetimes of 2–5 hr. The median per-cell flash rate is of the order of 3 per minute, and the median cell nearest neighbor range is 30 km (Boccippio et al., 2000). Assuming that the high electric field areas in the cloud are roughly 1% of the single-cell cloud coverage, we approximate the relevant area and time interval as  $\pi(5 \text{ km})^2 \times 1\% \times 20 \text{ s} \approx 15 \text{ km}^2 \text{ s}$ . Note that the radial extension of an EAS is much smaller than 1 km. Comparing the typical occurrence rates of lightning inception to the cosmic ray fluxes in equation (3), we conclude that we only need to study cosmic rays with energies up to  $10^{17}$  eV. While showers below  $10^{15}$  eV have even higher occurrence rates, we will see in our later analysis (cf. Figure 8) that their generated instantaneous seed electron density is insignificant. We therefore focus on cosmic ray energies between  $10^{15}$  and  $10^{17}$  eV.

## 3. Methodology

### 3.1. Simulations

Simulations of the EASs are performed with the Monte Carlo software package CORSIKA (Heck et al., 1998). CORSIKA acts as a steering code, where the user can select particle models. In this study we use the state-of-the-art high-energy hadronic interaction model QGSJET-II (Ostapchenko, 2006), and for the low-energy interaction (below TeV) we use FLUKA (Battistoni et al., 2007). When not described below, the standard settings are used, such as the implementation of the geomagnetic field. The full settings are described by Heck et al. (1998). We do not use the thinning option (simulating less particles with a higher particle weight), and we follow particles to their lowest energy threshold recommended in the software, which is 50 keV for electrons, positrons, and photons. We thus decouple the system and calculate the seed electrons as described in section 2.3.

In section 2.5 we argued that the relevant energy range of the primary cosmic rays is  $10^{15}$  to  $10^{17}$  eV. This energy range is divided into 99 equal intervals of  $10^{15}$  eV, meaning that the first interval is  $[1, 2] \times 10^{15}$  eV and the last interval (the 99th) is  $[99, 100] \times 10^{15}$  eV. Within each interval the primary energy  $E$  should be sampled randomly with a probability proportional to  $E^{-3}$ , according to equation (2). However, for better statistics of the rare showers with high cosmic ray energies, we have performed importance sampling, that is, oversampling the tail of the distribution, with a probability proportional to  $E^{-1}$ ; this is undone later. The number of simulations per energy interval of  $10^{15}$  eV is given in Figure 7, where the blue line represents the distribution if all EASs were sampled as  $E^{-3}$ . The inclination of the cosmic ray is sampled randomly, uniform per solid angle, up to a zenith angle of  $70^\circ$ , bound by the choice of using a horizontally geometrical atmosphere

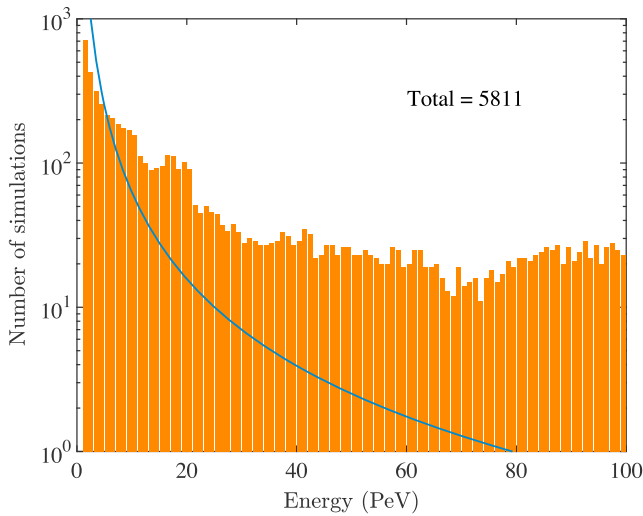


**Figure 7.** Overview of performed simulations. In total we used 125,000 CPU hours to compute 5,811 extensive air showers. The blue line represents the distribution if sampled as  $E^{-3}$ . We have performed importance sampling, that is, oversampling the tail of the distribution, for higher accuracy. The energy scale is 1 PeV =  $10^{15}$  eV.

(no curvature and no humidity); furthermore, the simulation results support the physical expectation that rays with larger incident angle do not penetrate so deep into the atmosphere. The primary cosmic rays start at 100-km altitude, high enough that previous collisions with atmospheric particles are negligible. The density profile is the U.S. standard atmosphere. In this study we only inject protons. Heavier cosmic particles do exist but are expected to produce similar showers.

For each shower we first retrieve at altitudes of 5 to 13 km, in steps of 1 km, the full output (particle ID, momentum, position, and arrival time) of each particle passing the hypothetical detector at that altitude. We only simulate down to 5 km for computational reasons, as in CORSIKA all particles are followed down to the lowest observational level. We postprocess this detailed data by counting the numbers  $\mathcal{N}_{R_1}$ ,  $\mathcal{N}_{R_2}$ , and  $\mathcal{N}_{R_3}$  of electrons and positrons (above 50 keV) that have passed the disk with radius  $R_1 = 10$  cm,  $R_2 = 1$  m, and  $R_3 = 10$  m around the shower axis at the given altitudes. These data can be retrieved from the supplementary file CORSIKA-results.txt. After processing, the detailed output is deleted due to memory constraints. We only postprocess electrons and positrons, independently of energy and arrival time due to the following considerations (some were already mentioned in section 2.3):

- The most abundant species in an EAS are photons, electrons, and positrons, in proportion of roughly 100:10:9. The ionization cross section, that is, the probability to produce low energetic electrons, is proportional to roughly  $1:10^6:10^6$ . This means that although photons are roughly 10 times more abundant, their ability to produce low-energy electrons is much lower and thus their contribution is negligible.
- For the energies considered in modeling EASs, electrons and positrons produce almost an equal amount of low-energy ionizations. Thus, we can sum the contributions of electrons and positrons.
- The amount of low-energy seed electrons created by impact ionization by the EAS electrons and positrons (with energies above 1 MeV) is almost independent of this energy; see the friction curve in Figure 5. Therefore, the generation rate of seed electrons is proportional to the number of EAS electrons and positrons, independently of the energy of the EAS particles.
- The spread between the first EAS particle to arrive at an altitude and the slowest 1% is of the order of subnanoseconds, well within the uncertainty introduced by the other approximations (such as the friction to electron yield; see the end of section 2.3). Therefore, we can integrate the number of particles over time.

To extract particle densities at disk radii other than 10 cm, 1 m, or 10 m, we employ the NKG function, named after Kamata and Nishimura (1958) and Greisen (1960); it can be used for a simple approximation of the lateral distribution of electromagnetic particles, that is, electrons and positrons. It allows us to interpolate and extrapolate from the simulation results at the given three radii to other observables. The NKG function in cylindrical coordinates with radius  $r$  from the core center and with angle  $\phi$  at an altitude  $z$  is given by

$$\frac{d^2 \mathcal{N}(z)}{r dr d\phi} = \mathcal{N}(z) \frac{1}{2\pi R_m^2} \frac{\Gamma(4.5 - s)}{\Gamma(s)\Gamma(4.5 - 2s)} \left(\frac{r}{R_m}\right)^{s-2} \left(1 + \frac{r}{R_m}\right)^{s-4.5}, \quad (4)$$

where  $\Gamma$  is the Euler function,  $s = s(z)$  is a fitting parameter (also known as the age parameter), and  $R_m$  is the Moliere radius. The age parameter correlates with the longitudinal state of development, hence the shower “age.” EASs start typically with a hadron, where the NKG function can be extended to include a radial dependence of the age parameter. This would be done by using the so-called lateral age  $s_{\perp}(z, r)$  (Apel et al., 2006; Bourdeau et al., 1980, and references therein). But we will approximate the lateral shape of the inner core (i.e.,  $r \leq 10$  m) just by using the single age parameter  $s(z)$  in equation (4).

By integrating the NKG function over the area of a disk with radius  $R$  (note that inclined showers form an ellipse shape in a vertical plane, but we evaluate a disk for all showers), we get for the flux of electrons and positrons through this disk

$$\mathcal{N}_R(z) = \mathcal{N}(z) \frac{\Gamma(4.5 - s)}{\Gamma(1 + s)\Gamma(4.5 - 2s)} \left(\frac{R}{R_m}\right)^s {}_2F_1(4.5 - s, s, 1 + s, -R/R_m). \quad (5)$$

Here  ${}_2F_1$  is the ordinary hypergeometric function.

For each simulated EAS event and for each observation altitude, we have determined the three parameters  $\mathcal{N}$ ,  $s$  and  $R_m$  in equation (5) from the three fluxes  $\mathcal{N}_{R_i}$  numerically with high precision ( $|\text{error}| < 10^{-12}$ ). Only for the showers that had an empty inner core  $\mathcal{N}_{R_1} = 0$ , the unknowns were fitted with a least  $\chi^2$  fit.

### 3.2. Probability Analysis

In this subsection we derive the probability distribution for the maximal strength of an EAS within a given system size  $A \cdot T$  (see illustration in Figure 6), based on the statistical data from the EAS simulations. The maximal strength is evaluated as the maximum over the strengths of all air showers within the system size. The strength of an EAS will be characterized by different observables, like the particle number passing through a disc of given radius, or the radius where a given particle density is reached. We now derive a general expression for an observable  $y$  in an EAS. We assume that  $y$  is a positive quantity  $y \geq 0$ .

For a given system size  $A \cdot T$ , the average number  $\bar{k}$  of cosmic rays in the relevant energy range of  $10^{15}$  to  $10^{17}$  eV is

$$\bar{k} = \frac{6.5 A \cdot T}{\text{km}^2 \text{ s}} \quad (6)$$

according to equation (3).

As already said in section 2.2, EASs happen at uncorrelated places in space and time, and the created free electron density is of short duration; thus, the showers should be considered as independent, nonoverlapping, and identically distributed events. Therefore, the number  $k$  of relevant EASs is a discrete random variable and Poisson distributed

$$\mathbf{p}_{\bar{k}}(k) = \frac{\bar{k}^k}{k!} e^{-\bar{k}}. \quad (7)$$

Now let  $y$  be an observable of interest of an EAS, as said above. The value of  $y$  in the  $i$ th EAS is denoted as  $y_i$ . The maximum over an ensemble  $\{y_i\}_{i=1, \dots, k}$  of  $k$  EAS depends on  $k$  and on the probability distribution of  $y$ . A cumulative distribution function is defined as the integral over all  $P(y)$  with  $y \leq m$ . The cumulative distribution functions  $\mathbf{P}_1(y_i \leq m)$  of one EAS and  $\mathbf{P}_k(\max_{i=1, \dots, k} \{y_i\} \leq m)$  of an ensemble of  $k$  EASs are related through

$$\mathbf{P}_k \left( \max_{i=1, \dots, k} \{y_i\} \leq m \right) = \prod_{i=1}^k \mathbf{P}_1(y_i \leq m) = \mathbf{P}_1(y \leq m)^k. \quad (8)$$

As the number of EASs within the system size can vary, we have to take the weighted sum over  $k$  to determine the probability distribution of a maximal outcome  $\max(y)$  for given average number  $\bar{k}$  of cosmic rays:

$$\mathcal{P}_{\bar{k}}(\max(y) \leq m) = \sum_{k=0}^{\infty} \mathbf{p}_{\bar{k}}(k) \mathbf{P}_k \left( \max_{i=1, \dots, k} \{y_i\} \leq m \right), \quad (9)$$

$$= e^{-\bar{k}} \sum_{k=0}^{\infty} \frac{(\bar{k} \mathbf{P}_1(y \leq m))^k}{k!}. \quad (10)$$

$$= e^{-\bar{k}} e^{\bar{k} \mathbf{P}_1(y \leq m)} = e^{-\bar{k} \mathbf{P}_1(y > m)}. \quad (11)$$

For equation (10), we used equations (7) and (8), and the fact that  $\mathbf{P}_0(\max_i \{y_i\} \leq m) = 1$  for any  $m \geq 0$ , as the density in a nonoccurring shower equals 0. (We note that equation (11) shows clearly that the function  $\mathcal{P}_{\bar{k}}(\max(y) \leq m)$  is a probability distribution with values between 0 and 1.)

Here  $\mathbf{P}_1(y \leq m)$  is the cumulative probability distribution function that  $y \leq m$  in a single air shower; it can be directly evaluated from our data. And  $\mathcal{P}_{\bar{k}}(\max(y) \leq m)$  is the cumulative probability distribution function that the maximum of  $y$  is smaller or equal  $m$  in an ensemble of air showers with given average number  $\bar{k}$  of cosmic rays.

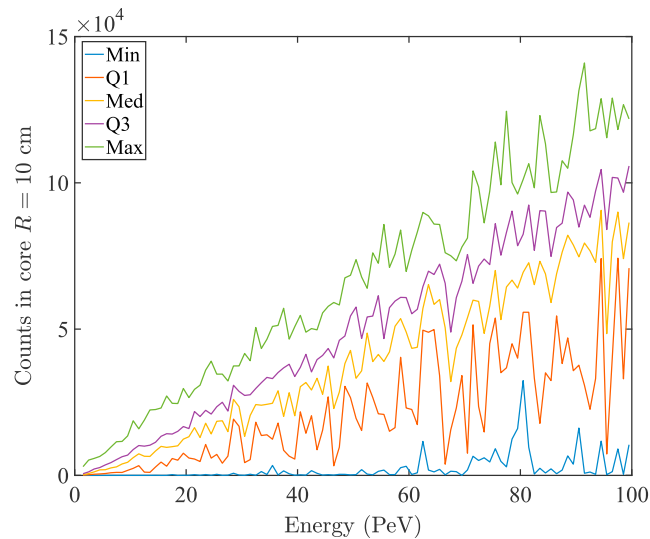


**Figure 8.** Stochastic distribution of the simulated number of EAS electrons and positrons per shower passing through a disc of 10-cm radius at 8-km altitude as a function of the energy of the primary particle. The five lines indicate a boxplot: the minimum value, the first quartile (25%), the median, the third quartile (75%), and the maximum value.

### 3.3. Reversal of the Importance Sampling

When  $P_1(y \leq m)$  is calculated empirically from the simulation data, the importance sampling has to be reversed. From the simulation results we resample with the correct  $E^{-3}$  distribution by drawing samples repeatedly from an energy bin. Practically, low-energy samples will thus enter the resampled distribution multiple times. In this way the set of 5,811 samples is enlarged to a new empirically resampled set of about  $10^7$  samples. Finally, a proper prefactor ensures the proper cosmic ray flux of equation (2).

## 4. Results

### 4.1. A First View on the Data

We have used 125,000 CPU hours to compute 5,811 EASs created by an incident high-energy proton, and we have processed 150 TB of binary data. We have recorded the number of electrons and positrons with energies above 50 keV passing through three core sizes (with radii of 10 cm, 1 m, and 10 m) at nine observational altitudes (5 to 13 km), as described in section 3. These are the EAS particles or ionizing flux, as described in section 2.3. These data are permanently stored and available on <https://doi.org/10.17026/dans-xcg-h326>. As an example, in Figure 8 the variation of the raw data for a core size of 10-cm radius at 8-km altitude is

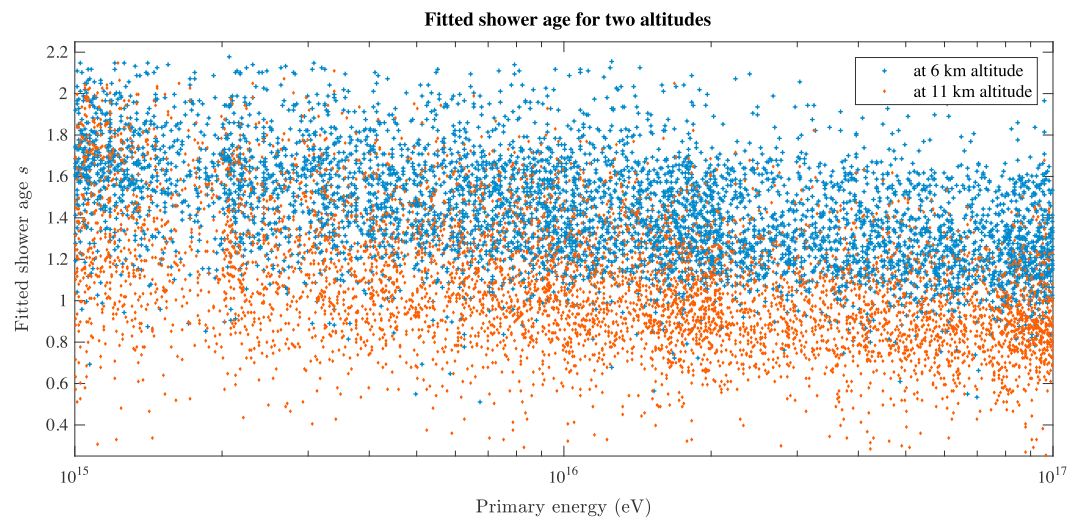


**Figure 9.** Fitted shower age at an altitude of 6 km (blue cross) and 11 km (red diamond).

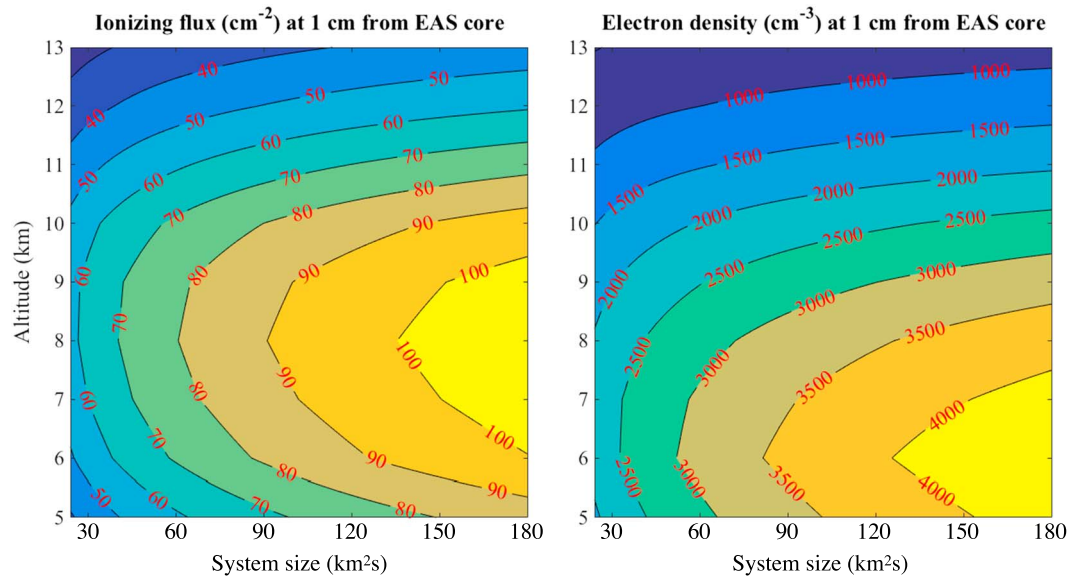


**Figure 10.** (left panel) Ionizing flux of EAS electrons and positrons, hence with energies above 50 keV, at 1 cm from the shower axis as a function of altitude and system size. The flux in units of  $\text{cm}^{-2}$  is indicated with color coding and level lines. The largest flux is plotted that can be expected in any of the passing EAS with probability 1/2. (right panel) Seed electrons, that is, free electrons with energies in the eV range plotted in the same manner. An example on how to read these plots: In a system size of  $30 \text{ km}^2 \text{ s}$  at 6-km altitude, a seed electron density of at least  $2,500 \text{ cm}^{-3}$  at 1 cm from the shower axis occurs with probability 1/2 somewhere in the system size. EAS = extensive air shower.

presented. We see the linear trend with energy; that is, the number of EAS particles per shower scales roughly linearly with the energy of the primary particle. However, the variation also increases and we see that the 25% largest showers created by a 50-PeV particle have a denser core than the 25% smallest showers created by a 100-PeV particle; this reflects the observation in Figure 3d that not only primary energy is important but that a full energy interval should be analyzed.

The first step in the postprocessing is a fitting to the integrated NKG function (equation (5)) for the three unknowns ( $\mathcal{N}$ ,  $s$ , and  $R_m$ ) for each shower and each altitude. In Figure 9 the distribution of fitted shower ages is shown for 6- and 11-km altitude as a function of energy. The large variation at each energy displays the large shower-to-shower fluctuations, as introduced in section 2.2. Two trends are visible. First, showers at 6-km altitude are older (i.e., they have a larger age parameter) than those at 11-km altitude. This is natural because showers evolve downward. Second, at the same altitude the showers tend to be younger (i.e., to have a smaller age parameter) for higher primary energies. This is also expected as the higher the primary energy of the cosmic ray, the deeper it can penetrate into the atmosphere before starting the EAS.

The integrated NKG function is used to approximate the lateral profile. There are multiple nonequivalent ways to sort a lateral profile in strength. One possibility is to look at the probability of very high seed electron densities in the center of the shower. Another possibility is to look at the probability of very large transversal extensions of the shower core for a given seed electron density. Both perspectives are relevant for discharge inception in thunderclouds and are discussed in more detail in section 5. Below the results in both perspectives are given.

#### 4.2. Probability of High Electron Densities at Given Radius

Now we analyze the ionizing flux of EAS particles (electrons and positrons with energies above 50 keV) and the density of seed electrons (with energies in the eV range) at 1 cm from the center of the shower.

The largest ionizing flux to be expected in any of the showers within the system size is calculated by evaluating equation (10) empirically with the simulation data. The result depends on the altitude in the atmosphere and on the considered system size through the parameter  $\bar{k}$ . The sum over  $k$  in equation (10) is evaluated up to  $2\bar{k}$  which is tested to be a sufficient approximation. The left panel in Figure 10 shows the median of the distribution function of the maximal ionizing flux as a function of altitude and system size  $A \cdot T$  (where the median is the value with  $\mathcal{P}_{\bar{k}} = 1/2$ ). The rarer the event (i.e., the larger the evaluated system size), the larger

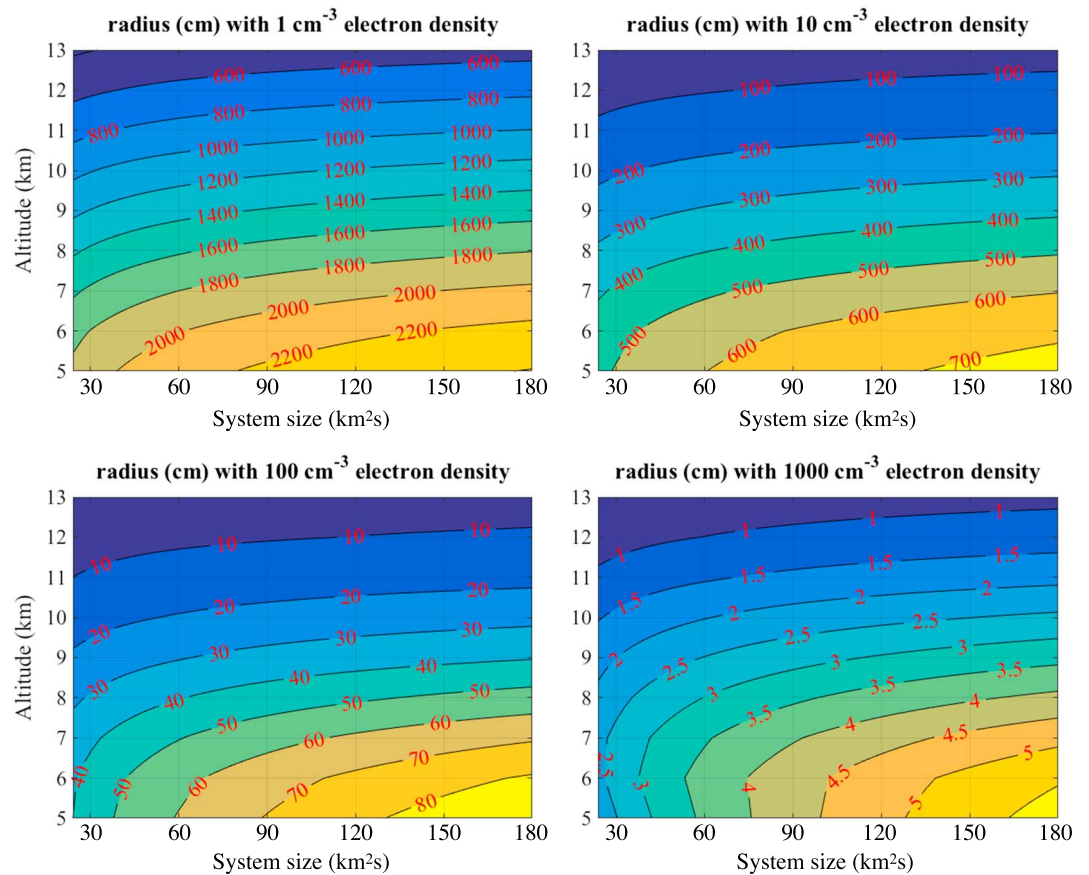


**Figure 11.** Distance from the shower axis in centimeters (color coded and with level lines) where the seed electron density is 1, 10, 100, or 1,000  $\text{cm}^{-3}$  in the different panels. The distance is plotted as a function of altitude and system size. An example on how to read these plots: At 5-km altitude a seed electron density of at least  $100 \text{ cm}^{-3}$  (see lower left panel for this density) at a radius of 70 cm from the shower axis occurs somewhere within a system size of  $90 \text{ km}^2\text{s}$  with probability 1/2.

the ionizing flux that can be expected in the shower of maximal strength. For all system sizes, the ionizing flux is largest at about 8-km altitude and decreases for higher or lower altitudes.

The right panel in Figure 10 shows the seed electron density at 1 cm from the shower axis as a function of altitude and system size; it is calculated by multiplying the ionizing flux with the average yield of seed electrons given in equation (1). Because the yield is smaller for smaller air densities (i.e., for higher altitudes), we see that the maximum of the seed electron density is at lower altitude than the maximum of the ionizing flux. For an EAS in a system size  $A \cdot T = 120 \text{ km}^2 \text{ s}$ , a free electron density of  $4,000 \text{ cm}^{-3}$  can be expected at around 6-km altitude. We also notice that the contour of  $1,000 \text{ cm}^{-3}$  tends to become independent of the system size for large system sizes near 13-km altitude. This can be expected because a more energetic primary particle will penetrate deeper into the atmosphere; though it will create a larger seed electron density over its whole path, it will do so only at lower altitude.

#### 4.3. Probability of Large Shower Radii With Given Electron Densities

In this subsection we find the probability of large radii of the EAS core with given electron densities. Now we sort the simulation data according to the radius about the shower core where the seed electron density equals 1, 10, 100, and  $1,000 \text{ cm}^{-3}$ , and the results are plotted in Figure 11 as a function of altitude and system size.

We notice that when increasing the electron density by an order of magnitude, the median of the largest inclosing radius decreases by an order of magnitude. We see a clear trend that the EAS core is wider at lower altitudes. As it should, the 1-cm contour line of the right panel in Figure 11 is identical to the  $1,000 \text{ cm}^{-3}$  density contour line in the right panel of Figure 10 because at this line both perspectives are equivalent. The core radius for high altitudes (say above 9 km) hardly changes for rarer events (i.e., for larger system sizes),

implying that it is not possible to get much larger extensions even for much rarer events. For altitudes above 5 km, system sizes up to 180 km<sup>2</sup>s, and seed electron densities of 1,000 cm<sup>-3</sup>, the median of the radius is smaller or equal 6 cm.

## 5. Discussion

### 5.1. Streamer Inception From Single Hydrometers

As said in section 1, streamer initiation in thunderclouds requires three ingredients (Dubinova et al., 2015): the thundercloud electric field, a hydrometeor (a droplet or ice particle), and free electrons. In this work we focus only on the third ingredient and calculate the median of the maximal seed electron density in the thundercloud system (ignoring avalanching effects in the local electric field). Discharge inception simulations in the literature typically use orders of magnitude larger initial electron densities than justified by our present analysis. In the simulations of Liu et al. (2012) and Sadighi et al. (2015) a seed electron density of 10<sup>11</sup> and 2 × 10<sup>9</sup> cm<sup>-3</sup> is taken, respectively, while Figure 10 shows that the maximal density does not exceed 5 × 10<sup>3</sup> cm<sup>-3</sup> even for very rare EASs, and that these very high densities only occur in very thin cores; see Figure 11. Sadighi et al. (2015) justify the large initial background density by a preexisting corona discharge. They refer to the work of Sin'kevich and Dvogyuk (2014) where the number of corona discharges due to hydrometeor collisions are calculated. But the point is that the initiation of a corona discharge and of a streamer discharge is the very same process. Both need the three ingredients quoted above, including initial free seed electrons to start. Thus, arguing that the initial electrons for one discharge come from another discharge does not solve the problem.

Babich et al. (2016, 2017) and Dubinova et al. (2015) use an initial density in their fluid model, but argue that only a single electron was needed. They differ in their assumption on the required ionization integral of the Meek criterion to start a positive streamer near a hydrometeor, but that is outside the scope of this work. Important here is that Babich et al. (2016, 2017) just postulate that there is a free electron available, either by background cosmic ray flux or by cloud charge fluctuations, but they do not calculate how frequently this occurs. Dubinova et al. (2015) calculate a seed electron density by requiring that a free electron on average survives the path to the hydrometeor rather than attaching to an oxygen molecule along the way, which yields a density of 100 cm<sup>-3</sup> for a given size and shape of the hydrometeor and for a given background electric field and altitude. They performed a statistical analysis of 297 EASs with primary particle energies from 5 × 10<sup>16</sup> to 5 × 10<sup>17</sup> eV (without importance sampling) to determine how likely such an electron density is. The current work explains how this analysis is done, provides a much better statistics and analyzes a larger energy range of cosmic particles between 10<sup>15</sup> and 10<sup>17</sup> eV.

Definitely at least one seed electron is needed for discharge inception, but more is always better, as it softens the Meek criterion (Babich et al., 2016, 2017; Cai et al., 2017; Dubinova et al., 2015). In other words, a larger initial number of electrons will soften the requirement for the other two ingredients, the value of the thundercloud electric field or the properties of the hydrometeor, such as size and sharpness (Dubinova et al., 2015) or net charge (Babich et al., 2016, 2017; Cai et al., 2017). However, our results presented here do not give a lot of room for a large increase of the electron density. Figure 10 and the lower right panel of Figure 11 show that a density of a few times 1,000 cm<sup>-3</sup> is possible, but only in a very limited core radius. To find a hydro-meteor with the right size and shape probably limits the inception probability more than the logarithmic dependence on the electron density. When the electron density is too low for a given hydrometeor, field and altitude, inception becomes a random process with a probability proportional to the seed electron density. For further details, we refer to the PhD thesis of the first author (Rutjes, 2018) and a forthcoming paper submission.

### 5.2. Simultaneous Triggering of a System of Streamers by an EAS

When considering the simultaneous triggering of a system of streamers as observed by Rison et al. (2016), it is crucial to have enough free electrons over a sufficiently large area at the same moment in time. In the hypothesis that a system of multiple streamers from multiple hydrometeors are necessary to start lightning, in agreement with the detailed observations of Narrow Bipolar Events (NBEs) (Rison et al., 2016), the EAS core needs to be sufficiently extended. Similar observations have actually been made earlier by Defer et al. (2001) and Bruning et al. (2010) in cases where lightning did not start, as an indication of attempted breakdown; Rison et al. (2016) interpret this as a system of streamers which is triggered but not capable of developing to a full-fledged lightning stroke.

As Rison et al. (2016) discuss, to explain the strong sphericity, multiple streamers side-by-side are necessary and the observations show a relatively large lateral extension of around 50 to 100 m. Examining closely NBE3 from Rison et al. (2016, see their supplementary Figure 9), we see that the first two data points recorded span horizontally 129 m (and vertically 58 m), but the time between these events is only  $3.8 \times 10^{-7}$  s. They thus cannot be causally related, as they are outside of each other's light cone. We see this as evidence that they must be triggered together within a simultaneous event, a fast event with a time scale of less than a microsecond. Even considering both end points of the error bars of the position (see supplementary Figure 18 of NBE3 from Rison et al., 2016), the speed would be much faster than is typical for streamers and the propagation direction would be perpendicular to the streamer propagation direction after initiation, that is, to the direction of the electric field. In other words, when the downward propagation is streamer-like and driven by a vertical electric field, the horizontal propagation would be much faster and perpendicular to the field, which is not how discharges typically propagate. We rather suggest that all first four points of the NBE3 observation are triggered simultaneously by an EAS event, though this cannot be proven from the data presented by Rison et al. (2016). For the other two NBEs presented by Rison et al. (2016), the evidence is harder to retrieve, as data points in the presented plots overlap, but for NBE1 it is still convincing. Studying closely NBE1 (see their supplementary Figure 7), we see that the first two events are separated vertically by 87 m in only  $1.8 \times 10^{-7}$  s (it was not clear how much the azimuth angle was). Thus, they are also outside each other's light cone or at least much faster than streamers and must therefore be triggered by the same event, presumably by one extreme EAS event.

To trigger a system of streamers by an EAS event, one should analyze the probability within an event box (as introduced by Dubinova et al., 2015) large enough for the inception of multiple streamers. The top area  $A$  of the event box times the waiting time  $T$  defines the probability of a rare event (i.e., the availability of an extreme EAS with a low occurrence rate). From all NBE results presented by Rison et al. (2016) we estimate that the EAS core radius must be at least of the order of tens of meters. From Figure 11 we find that the maximally expected electron density for such large core radii is of the order of  $1 \text{ cm}^{-3}$ .

This means that discharge inception near each hydrometeor (with extensions in the mm range) is a stochastic process with probability proportional to the electron density: Is there an electron at the right position relative to the hydrometeor such that it can drift toward it rather than to attach to oxygen, and that it can create a sufficiently strong avalanche to generate a streamer discharge from the hydrometeor? But if the field is high enough, and if there is a sufficient density of hydrometeors with appropriate shape, an EAS could trigger the simultaneous start of a volume system of streamers.

## 6. Conclusions and Outlook

We have calculated the probability of high densities of seed electrons in the eV range, which can be expected in thunderclouds during a short time span due to extensive air showers. The main results of our rare event analysis are presented in Figures 10 and 11; they give the maximal density of seed electrons that can be expected at a given altitude at some place in space and time within the system size  $A \cdot T$  (see Figure 6). In the figures we present the maximal density at 1 cm from the EAS core and the maximal radius where an electron density of 1, 10, 100, or  $1,000 \text{ cm}^{-3}$  can be expected. This initial free electron density can be used when studying streamer initiation in the context of lightning inception. It is an input for the analysis of streamer inception from a single hydrometeor as analyzed by Dubinova et al. (2015), though the single electron needed could also be produced by a weaker cosmic ray or a radioactive decay. However, when lightning starts by a volumetric system of streamers (Rison et al., 2016), it is crucial that enough free electrons are created simultaneously within a limited volume and time span.

The measurements of Rison et al. (2016) reveal that the first few radiowave emitting discharges must be triggered simultaneously, as some of them lie outside of each other's light cone; in other cases the information between the first few discharges must travel much faster than streamers do. We suggest that this is evidence that they are initiated simultaneously by one EAS event, as we discuss in section 5.2. The measurements of Rison et al. (2016) reveal further that the lateral width of the volumetric system of streamers is of the order of tens of meters, which according to our results implies initiation from electron densities as low as  $1 \text{ cm}^{-3}$ , demanding a stochastic approach to streamer initiation as sketched above.

**Acknowledgments**

C. R. and T. N. G. T. acknowledge funding by FOM project 12PR3041 in The Netherlands. We acknowledge Jeroen Witteveen († 2015) for the constructive discussions and contributions on the probability analysis. We also thank the 3 referees, in particular Dr. Michael McCarthy from the University of Washington for extensive and constructive comments. All the input data used are listed in the references or available on the website (<https://www.ikp.kit.edu/corsika/>). The results CORSIKA-results.txt of the 5811 simulations are permanently stored and available on <https://doi.org/10.17026/dans-xcg-h326>; they contain energy, inclination, and altitude of first interaction of each simulated ray, as well as the generated ionizing flux of electrons and positrons with energy above 50 keV within a radius of 10, 100, and 1,000 cm and infinity at 13, 12, . . . , 5 km altitude.

**References**

Apel, W., Badea, A., Bekk, K., Bercuci, A., Blümer, J., Bozdog, H., et al. (2006). Comparison of measured and simulated lateral distributions for electrons and muons with KASCADE. *Astroparticle Physics*, 24(6), 467–483. <https://doi.org/10.1016/j.astropartphys.2005.10.001>

Babich, L. P., Bochkov, E. I., Kutsyk, I. M., Neubert, T., & Chanrion, O. (2016). Positive streamer initiation from raindrops in thundercloud fields. *Journal of Geophysical Research: Atmospheres*, 121, 6393–6403. <https://doi.org/10.1002/2016JD024901>

Babich, L., Bochkov, E., & Neubert, T. (2017). The role of charged ice hydrometeors in lightning initiation. *Journal of Atmospheric and Solar-Terrestrial Physics*, 154, 43–46. <https://doi.org/10.1016/j.jastp.2016.12.010>

Battistoni, G., Cerutti, F., Fasso, A., Ferrari, A., Muraro, S., Ranft, J., et al. (2007). The fluka code: Description and benchmarking. In *Hadronic Shower Simulation Workshop(AIP Conference Proceedings Volume 896)*, 896, NY, pp. 31–49. <https://doi.org/10.1063/1.2720455>

Boccippio, D. J., Goodman, S. J., & Heckman, S. (2000). Regional differences in tropical lightning distributions. *Journal of Applied Meteorology*, 39(12), 2231–2248. [https://doi.org/10.1175/1520-0450\(2001\)040<2231:RDITLD>2.0.CO;2](https://doi.org/10.1175/1520-0450(2001)040<2231:RDITLD>2.0.CO;2)

Bourdeau, M. F., Capdevielle, J. N., & Procureur, J. (1980). The lateral age parameter in extensive air showers. *Journal of Physics G: Nuclear Physics*, 6(7), 901. <https://doi.org/10.1088/0305-4616/6/7/013>

Bruning, E. C., Rust, W. D., MacGorman, D. R., Biggerstaff, M. I., & Schuur, T. J. (2010). Formation of charge structures in a supercell. *Monthly Weather Review*, 138(10), 3740–3761. <https://doi.org/10.1175/2010MWR3160.1>

Cai, Q., Jánský, J., & Pasko, V. P. (2017). Initiation of positive streamer corona in low thundercloud fields. *Geophysical Research Letters*, 44, 5758–5765. <https://doi.org/10.1002/2017GL073107>

Cole, A. (1969). Absorption of 20-eV to 50,000-eV electron beams in air and plastic. *Radiation Research*, 38(1), 7–33. <https://doi.org/10.2307/3572707>

Defer, E., Blanchet, P., Théry, C., Laroche, P., Dye, J. E., Venticinque, M., & Cummins, K. L. (2001). Lightning activity for the July 10, 1996, storm during the Stratosphere-Troposphere Experiment: Radiation, Aerosol, and Ozone-A (STERAO-A) experiment. *Journal of Geophysical Research*, 106(D10), 10,151–10,172. <https://doi.org/10.1029/2000JD900849>

Dubnova, A., Rutjes, C., Ebert, U., Buitink, S., Scholten, O., & Trinh, G. T. N. (2015). Prediction of lightning inception by large ice particles and extensive air showers. *Physical Review Letters*, 115(1), 015002. <https://doi.org/10.1103/PhysRevLett.115.015002>

Dwyer, J. R., & Babich, L. P. (2011). Low-energy electron production by relativistic runaway electron avalanches in air. *Journal of Geophysical Research*, 116, A09301. <https://doi.org/10.1029/2011JA016494>

Gaisser, T. K., Engel, R., & Resconi, E. (2016). *Cosmic rays and particle physics*. Cambridge: Cambridge University Press.

Gallimberti, I. (1979). The mechanism of the long spark formation. *Journal de Physique Colloques*, 40(C7), 193. <https://doi.org/10.1051/jphyscol:19797440>

Greisen, K. (1960). Cosmic ray showers. *Annual Review of Nuclear Science*, 10(1), 63–108. <https://doi.org/10.1146/annurev.ns.10.120160.000431>

Heck, D., Schatz, G., Knapp, J., Thouw, T., & Capdevielle, J. (1998). Corsika: A Monte Carlo code to simulate extensive air showers. Karlsruhe, Germany: Forschungszentrum Karlsruhe GmbH.

Jesse, W. P., & Sadauskis, J. (1955). Ionization in pure gases and the average energy to make an ion pair for alpha and beta particles. *Physical Review*, 97, 1668–1670. <https://doi.org/10.1103/PhysRev.97.1668>

Kamata, K., & Nishimura, J. (1958). The lateral and the angular structure functions of electron showers. *Progress of Theoretical Physics Supplement*, 6, 93. <https://doi.org/10.1143/PTPS.6.93>

Knoll, G. F. (2010). *Radiation detection and measurement*. New York: John Wiley & Sons.

Lafebre, S., Engel, R., Falcke, H., Horandel, J., Huege, T., Kuijpers, J., & Ulrich, R. (2009). Universality of electron-positron distributions in extensive air showers. *Astroparticle Physics*, 31, 243–254.

Lipari, P. (2016). Universality in the longitudinal development of cosmic ray showers. *Nuclear and Particle Physics Proceedings*, 279–281, 111–117. <https://doi.org/10.1016/j.nuclphysbps.2016.10.016>, Proceedings of the 9th Cosmic Ray International Seminar.

Liu, N., Kosar, B., Sadighi, S., Dwyer, J. R., & Rassoul, H. K. (2012). Formation of streamer discharges from an isolated ionization column at subbreakdown conditions. *Physical Review Letters*, 109(2), 025002. <https://doi.org/10.1103/PhysRevLett.109.025002>

Marshall, T. C., McCarthy, M. P., & Rust, W. D. (1995). Electric field magnitudes and lightning initiation in thunderstorms. *Journal of Geophysical Research*, 100(D4), 7097–7103. <https://doi.org/10.1029/95JD00020>

Marshall, T. C., Stolzenburg, M., Maggio, C. R., Coleman, L. M., Krehbiel, P. R., Hamlin, T., et al. (2005). Observed electric fields associated with lightning initiation. *Geophysical Research Letters*, 32, L03813. <https://doi.org/10.1029/2004GL021802>, L03813.

Ostapchenko, S. (2006). QGSJET-II: Towards reliable description of very high energy hadronic interactions. *Nuclear Physics B-Proceedings Supplements*, 151(1), 143–146. <https://doi.org/10.1016/j.nuclphysbps.2005.07.026>

Pancheshnyi, S. (2013). Effective ionization rate in nitrogen–oxygen mixtures. *Journal of Physics D: Applied Physics*, 46(15), 155201. <https://doi.org/10.1088/0022-3727/46/15/155201>

Patrignani, C., Richardson, P., Zenin, O., Zhu, R.-Y., Vogt, A., Pagan Griso, S., et al. Particle Data Group (2016). Review of particle physics, 2016–2017. *Chinese Physics C*, 40, 100001.

Rison, W., Krehbiel, P. R., Stock, M. G., Edens, H. E., Shao, X.-M., Thomas, R. J., et al. (2016). Observations of narrow bipolar events reveal how lightning is initiated in thunderstorms. *Nature Communications*, 7, 10721. <https://doi.org/10.1038/ncomms10721>

Rutjes, C. (2018). Modeling high energy atmospheric physics and lightning inception Eindhoven: Technische Universiteit Eindhoven. [https://pure.tue.nl/ws/portalfiles/portal/92383049/20180315\\_Rutjes.pdf](https://pure.tue.nl/ws/portalfiles/portal/92383049/20180315_Rutjes.pdf)

Sadighi, S., Liu, N., Dwyer, J. R., & Rassoul, H. K. (2015). Streamer formation and branching from model hydrometeors in subbreakdown conditions inside thunderclouds. *Journal of Geophysical Research: Atmospheres*, 120, 3660–3678. <https://doi.org/10.1002/2014JD022724>

Santos, J., Parente, F., & Kim, Y.-K. (2003). Cross sections for K-shell ionization of atoms by electron impact. *Journal of Physics B: Atomic, Molecular and Optical Physics*, 36(21), 4211.

Sin'kevich, A. A., & Dovgalyuk, Y. A. (2014). Corona discharge in clouds. *Radiophysics and Quantum Electronics*, 56(11), 818–828. <https://doi.org/10.1007/s11141-014-9484-y>

Stolzenburg, M., Marshall, T. C., Rust, W. D., Bruning, E., MacGorman, D. R., & Hamlin, T. (2007). Electric field values observed near lightning flash initiations. *Geophysical Research Letters*, 34, L04804. <https://doi.org/10.1029/2006GL028777>, L04804.

Stolzenburg, M., Rust, W. D., & Marshall, T. C. (1998). Electrical structure in thunderstorm convective regions: 3. Synthesis. *Journal of Geophysical Research*, 103, 14. <https://doi.org/10.1029/97JD03545>

Usoskin, I. G., Desorgher, L., Velinov, P., Storini, M., Flückiger, E. O., Büttikofer, R., & Kovaltsov, G. A. (2009). Ionization of the Earth's atmosphere by solar and galactic cosmic rays. *Acta Geophysica*, 57(1), 88–101. <https://doi.org/10.2478/s11600-008-0019-9>

Usoskin, I. G., & Kovaltsov, G. A. (2006). Cosmic ray induced ionization in the atmosphere: Full modeling and practical applications. *Journal of Geophysical Research*, 111, D21206. <https://doi.org/10.1029/2006JD007150>